# Updated results from the $\nu\_\tau$ appearance search in Nomad

P. Astier, D. Autiero, A. Baldisseri, M. Baldo-Ceolin, G. Ballocchi, M. Banner, G. Bassompierre, K. Benslama, N. Besson, I G. Bird, et al.

EUROPEAN LABORATORY FOR PARTICLE PHYSICS

CERN-EP-2000-049
March 17, 2000

# Updated Results from the $\nu_\tau$ Appearance Search in NOMAD

NOMAD Collaboration

P. Astier [n] D. Autiero [h] A. Baldisseri [r] M. Baldo-Ceolin [m]
G. Ballocchi [h] M. Banner [n] G. Bassompierre [a] K. Benslama [i]
N. Besson [r] I. Bird [h,i] B. Blumenfeld [b] F. Bobisut [m] J. Bouchez [r]
S. Boyd [t] A. Bueno [c,x] S. Bunyatov [f] L. Camilleri [h] A. Cardini [j]
P.W. Cattaneo [o] V. Cavasinni [p] A. Cervera-Villanueva [h,v]
G. Collazuol [m] G. Conforto [h,u] C. Conta [o] M. Contalbrigo [m]
R. Cousins [j] D. Daniels [c] H. Degaudenzi [i] T. Del Prete [p]
A. De Santo [h,p] T. Dignan [c] L. Di Lella [h] E. do Couto e Silva [h]
J. Dumarchez [n] M. Ellis [t] G.J. Feldman [c] R. Ferrari [o] D. Ferrère [h]
V. Flaminio [p] M. Fraternali [o] J.-M. Gaillard [a] E. Gangler [h,n]
A. Geiser [e,h] D. Geppert [e] D. Gibin [m] S. Gninenko [h,ℓ] A. Godley [t]
J.-J. Gomez-Cadenas [h,v] J. Gosset [r] C. Gößling [e] M. Gouanère [a]
A. Grant [h] G. Graziani [g] A. Guglielmi [m] C. Hagner [r]
J. Hernando [v] D. Hubbard [c] P. Hurst [c] N. Hyett [k] E. Iacopini [g]
C. Joseph [i] F. Juget [i] M. Kirsanov [ℓ] O. Klimov [f] J. Kokkonen [h]
A. Kovzelev [ℓ,o] A. Krasnoperov [a,f] V.E. Kuznetsov [f,h]
S. Lacaprara [m] C. Lachaud [n] B. Lakić [w] A. Lanza [o]
L. La Rotonda [d] M. Laveder [m] A. Letessier-Selvon [n] J.-M. Levy [n]
L. Linssen [h] A. Ljubičić [w] J. Long [b] A. Lupi [g] A. Marchionni [g]
F. Martelli [u] X. Méchain [r] J.-P. Mendiburu [a] J.-P. Meyer [r]
M. Mezzetto [m] S.R. Mishra [c,s] G.F. Moorhead [k] P. Nédélec [a]
Yu. Nefedov [f] C. Nguyen-Mau [i] D. Orestano [q] F. Pastore [q]
L.S. Peak [t] E. Pennacchio [u] H. Pessard [a] R. Petti [h,o] A. Placci [h]
G. Polesello [o] D. Pollmann [e] A. Polyarush [ℓ] B. Popov [f,n]
C. Poulsen [k] L. Rebuffi [m] J. Rico [x] C. Roda [h,p] A. Rubbia [h,x]

*( To be published in Physics Letters B)*

F. Salvatore [o] K. Schahmaneche [n] B. Schmidt [e,h] M. Sevior [k]
D. Sillou [a] F.J.P. Soler [h,t] G. Sozzi [i] D. Steele [b,i] M. Steininger [i]
U. Stiegler [h] M. Stipčević [w] Th. Stolarczyk [r] M. Tareb-Reyes [i]
G.N. Taylor [k] V. Tereshchenko [f] A. Toropin [ℓ] A.-M. Touchard [n]
S.N. Tovey [h,k] M.-T. Tran [i] E. Tsesmelis [h] J. Ulrichs [t]
L. Vacavant [i] M. Valdata-Nappi [d,y] V. Valuev [f,j] F. Vannucci [n]
K.E. Varvell [t] M. Veltri [u] V. Vercesi [o] J.-M. Vieira [i]
T. Vinogradova [j] F.V. Weber [c,h] T. Weisse [e] F.F. Wilson [h]
L.J. Winton [k] B.D. Yabsley [t] H. Zaccone [r] K. Zuber [e]
P. Zuccon [m]

[a] *LAPP, Annecy, France*
[b] *Johns Hopkins Univ., Baltimore, MD, USA*
[c] *Harvard Univ., Cambridge, MA, USA*
[d] *Univ. of Calabria and INFN, Cosenza, Italy*
[e] *Dortmund Univ., Dortmund, Germany*
[f] *JINR, Dubna, Russia*
[g] *Univ. of Florence and INFN, Florence, Italy*
[h] *CERN, Geneva, Switzerland*
[i] *University of Lausanne, Lausanne, Switzerland*
[j] *UCLA, Los Angeles, CA, USA*
[k] *University of Melbourne, Melbourne, Australia*
[ℓ] *Inst. Nucl. Research, INR Moscow, Russia*
[m] *Univ. of Padova and INFN, Padova, Italy*
[n] *LPNHE, Univ. of Paris VI and VII, Paris, France*
[o] *Univ. of Pavia and INFN, Pavia, Italy*
[p] *Univ. of Pisa and INFN, Pisa, Italy*
[q] *Roma Tre University and INFN, Rome, Italy*
[r] *DAPNIA, CEA Saclay, France*
[s] *Univ. of South Carolina, Columbia, SC, USA*
[t] *Univ. of Sydney, Sydney, Australia*
[u] *Univ. of Urbino, Urbino, and INFN Florence, Italy*
[v] *IFIC, Valencia, Spain*
[w] *Rudjer Bošković Institute, Zagreb, Croatia*
[x] *ETH Zürich, Zürich, Switzerland*
[y] *Now at Univ. of Perugia and INFN, Italy*

**Abstract**

Updated results from the appearance searches for $\nu_\mu \to \nu_\tau$ and $\nu_e \to \nu_\tau$ oscillations in the full NOMAD data sample are reported. The increased data and the use of more refined kinematic schemes for the $\nu_\tau$ CC selection allow a significant improvement of the overall sensitivity. The "blind analysis" of both the deep-inelastic and the low multiplicity samples yields no evidence for an oscillation signal. In the two-family oscillation scenario, this sets a 90% C.L. region in the $\sin^2 2\theta_{\mu\tau} - \Delta m^2$ plane which includes $\sin^2 2\theta_{\mu\tau} < 4.4 \times 10^{-4}$ at large $\Delta m^2$ and $\Delta m^2 < 0.8$ eV$^2/c^4$ at $\sin^2 2\theta_{\mu\tau} = 1$. The corresponding contour in the $\nu_e \to \nu_\tau$ oscillation hypothesis results in $\sin^2 2\theta_{e\tau} < 2.2 \times 10^{-2}$ at large $\Delta m^2$ and $\Delta m^2 < 6.5$ eV$^2/c^4$ at $\sin^2 2\theta_{e\tau} = 1$.

*Key words:* neutrino oscillations

## 1 Introduction

The $\nu_\tau$ appearance search for neutrino oscillations in NOMAD relies on the identification of $\nu_\tau$ charged-current (CC) interactions using kinematic criteria. Recent searches for $\nu_\mu \to \nu_\tau$ [1] and $\nu_e \to \nu_\tau$ [2] oscillations, based on about 950 000 $\nu_\mu$ CC interactions in the detector fiducial volume, yielded no evidence for oscillations.

In this letter we report a new search for $\nu_\mu \to \nu_\tau$ oscillations in the full NOMAD data sample collected during the 1995, 1996, 1997 and 1998 runs which corresponds to about 1 040 000 events with an identified muon and to about 1 350 000 $\nu_\mu$ CC interactions, given the combined trigger, vertex selection, and muon detection efficiency of about 77%. This analysis includes both deep inelastic (DIS) interactions and low-multiplicity events (LM). The enlarged data sample was supported by an increase in the number of the simulated Monte Carlo (MC) neutrino interactions with respect to Ref. [1], leading to a corresponding improvement in the kinematic selection of $\nu_\tau$ CC events and to a more accurate estimation of the different background sources. The analyses described in Ref. [1] were then replaced by more sensitive ones (see Sec. 4.4).

In the context of a two-flavour approximation, we then reinterpret the $\nu_\mu \to \nu_\tau$ result in terms of $\nu_e \to \nu_\tau$ oscillations, by assuming that any observed $\nu_\tau$ signal should come from the small $\nu_e$ component of the beam [2].

## 2 NOMAD detector

The NOMAD detector is described in Ref. [3]. Inside a 0.4 T magnetic field is an active target (2.7 tons) of drift chambers (DC), followed by a transition radiation detector (TRD) [4], a preshower detector (PS), and an electromagnetic calorimeter (ECAL) [5]. A hadron calorimeter (HCAL) and two muon stations are located just after the magnet coil.

The neutrino interaction trigger [6] consists of a coincidence between signals from two planes of counters located after the active target, in the absence of a signal from a large area system of veto counters in front of the NOMAD detector.

## 3 Neutrino beam and event samples

The estimated relative beam composition is $\nu_\mu : \bar{\nu}_\mu : \nu_e : \bar{\nu}_e = 1.00 : 0.061 : 0.0094 : 0.0024$, with average neutrino energies of 23.5, 19.2, 37.1, and 31.3 GeV, respectively [7]. For the analyzed data sample, it corresponds to about 34 000 $\bar{\nu}_\mu$ CC, 20 000 $\nu_e$ CC, and 2100 $\bar{\nu}_e$ CC interactions, and to a total of 485 000 neutral current (NC) interactions. Neutrinos are produced at an average distance of 625 m from the detector. The prompt $\nu_\tau$ component is negligible [8].

High statistics MC samples have been generated in order to estimate the background contributions from neutrino interactions. The size of the simulated samples exceeds the data sample by a factor of about 3 for $\nu_\mu$ CC interactions, 7 for $NC$ interactions, 10 for $\bar{\nu}_e$ CC and $\bar{\nu}_\mu$ CC interactions and 100 for $\nu_e$ CC interactions. In addition, about $10^5$ $\nu_\tau$ CC events have been generated for each $\tau^-$ decay channel. Details of these simulations can be found in Ref. [1].

## 4 Analysis principles

The search for $\nu_\tau$ CC interactions is performed by identifying the $\tau$ decays $e^-\bar{\nu}_e\nu_\tau$, $h^-(n\pi^0)\nu_\tau$ and $h^-h^+h^-(n\pi^0)\nu_\tau$, for a total branching ratio of 82.8%. Neutrino interactions in the active target are selected by requiring the presence of at least one track in addition to the $\tau$ decay products, having a common vertex in the detector fiducial volume. Quality cuts are then applied to ensure that the selected events are properly reconstructed. These requirements, based on approximate charge balance at the primary vertex and on the estimated momentum and energy errors, typically remove about 15% of the events. Events containing a primary track identified as a muon by the muon

stations are also rejected. The candidate particle or system of particles $\tau_{\rm V}$ consistent with being produced in $\tau$ decay is then identified and the associated hadronic system $H$ is built. The final discrimination between signal and background is achieved by using appropriate kinematic variables. For each $\tau$ decay mode two independent analyses are performed in the DIS and LM samples, which are separated by a cut on the total hadronic momentum $p^H$ at 1.5 GeV/c.

### *4.1 Kinematic variables*

The kinematic selection in each $\tau$ decay mode is based on a set of global variables which describe the general properties of the momenta of the candidate $\tau_{\rm V}$ and of the hadronic system $H$ in the laboratory frame. The proper sets of variables are selected from the following list:

- $E_{\rm vis}$, the total visible energy of the event.
- $\mathbf{p}^{\tau_{\rm V}}$ and $\mathbf{p}^H$, the total momentum of the *visible* tau decay product(s) and of the associated hadronic system respectively.
- $E^{\tau_{\rm V}}$ the total energy of the visible tau decay product(s).
- $y_{Bj}$, the ratio between $p^H$ and the total visible energy.
- $\mathbf{p}_T^{\tau_{\rm V}}$ and $\mathbf{p}_T^H$, the components of $\mathbf{p}^{\tau_{\rm V}}$ and $\mathbf{p}^H$ perpendicular to the neutrino beam direction.
- $\mathbf{p}_T^m$, defined as $-(\mathbf{p}_T^{\tau_{\rm V}}+\mathbf{p}_T^H)$ and interpreted as a measurement of the "missing" transverse momentum due to the neutrino(s) from $\tau$ decay.
- $p_{T\,||}^m$, the component of the missing transverse momentum parallel to the transverse momentum of the $\tau_{\rm V}$ candidate.
- $M_T$, the transverse mass (given by $M_T^2 = 4p_T^{\tau_{\rm V}} p_T^m \sin^2(\phi_{\tau_{\rm V} m}/2)$, where $\phi_{\tau_{\rm V} m}$ is the angle between $\mathbf{p}_T^{\tau_{\rm V}}$ and $\mathbf{p}_T^m$, when assuming massless decay product(s)). For true $\tau$ events, $M_T \leq m_\tau$, up to detector resolution and Fermi motion effects.
- $Q_T$, the component of $\mathbf{p}^{\tau_{\rm V}}$ perpendicular to the total visible momentum vector (including $\tau_{\rm V}$).
- $Q_{\rm Lep}$, the component of $\mathbf{p}^{\tau_{\rm V}}$ perpendicular to $\mathbf{p}^H$. Its function is very similar to $Q_T$, but it is more useful when $p^H$ is small.
- $\phi_{\tau_{\rm V} H}$, $\phi_{mH}$, the angles between $\mathbf{p}_T^H$ and $\mathbf{p}_T^{\tau_{\rm V}}$ and $\mathbf{p}_T^m$, respectively [9].
- Ratios $\rho_{\tau_{\rm V}}$, $\rho_H$ and $\rho_m$ of the transverse momenta $p_T^{\tau_{\rm V}}$, $p_T^H$ and $p_T^m$ and their sum $(p_T^{\tau_{\rm V}} + p_T^H + p_T^m)$.
- Ratios of linear combinations of the transverse momenta $\hat{\nu} = (p_T^{\tau_{\rm V}} - p_T^m)/p_T^H$ and $\hat{\mu} = (p_T^{\tau_{\rm V}} - p_T^H + p_T^m)/(p_T^{\tau_{\rm V}} + p_T^H + p_T^m)$.
- The asymmetry $p_T^{as} = (p_T^{\tau_{\rm V}} - p_T^H)/(p_T^{\tau_{\rm V}} + p_T^H)$.
- $\theta_{\nu T}$, the angle between the neutrino beam direction and the total visible momentum vector of the event.
- $\theta_{\nu H}$, the angle between the neutrino beam direction and the hadronic jet.

- $\theta_{\nu\tau_V}$, the angle between the neutrino beam direction and the $\tau_V$ momentum vector.
- $\theta_{\tau_V H}$, the angle between the hadronic jet and $\tau_V$.
- $\theta_{\tau_V h_i}$, the minimum angle between $\tau_V$ and any other primary track $h_i$ in the event.

In addition, variables describing the internal structure of the candidate $\tau_V$ can be used, where applicable, in order to increase background rejection.

### *4.2 Statistical analysis of data*

Since internal correlations within the chosen set of variables reduce the overall rejection power of individual cuts, variables are combined into global discriminating functions for each $\tau$ decay mode. An unbinned multi-dimensional likelihood ratio would give the optimal result. However, the available MC statistics and practical difficulties impose some approximations. For most channels the likelihood functions, $\mathcal{L}$, entering the likelihood ratio are built from one, two, three or four dimensional (1D, 2D, 3D, 4D) probability density functions (pdf), which in the following are denoted by a square bracket. The true likelihood function is then often approximated by the product of the considered pdf's (denoted by the product of the corresponding square brackets). Alternatively, in order to avoid the factorization approximation, a direct combination which takes into account residual correlations between the partial pdf's is used for the most sensitive channels. As is common practice, the logarithm of the final likelihood ratio, $\ln\lambda$, is used.

A different approximation is based on artificial neural networks (ANN) which receive the original set of variables as an input. A larger set of variables is generally required with this approach.

A likelihood fit to the tail of the final discriminating functions with separate signal and background contributions can increase the statistical power of the search. Since few events are expected in the relevant region, the likelihood fit is approximated by a binning which exploits any variation of the signal to background ratio along the tail of the distributions. The corresponding bins are then considered to be statistically independent.

### *4.3 Data simulator*

Our Monte Carlo simulator of $\nu$ interactions does not describe well enough the properties of the produced hadrons [3]. In order to reliably compute background rejections, based on the hadronic system, as large as $10^5$, the MC

results are corrected using a data simulator based on the data themselves [1]. We perform this correction by using a sample of $\nu_\mu$ CC events from the data, removing the *identified* muon, and replacing it with a MC-generated lepton $\ell$ of appropriate momentum vector, where $\ell$ can be a $\nu$, an $e^-$ or a $\tau^-$ decay. All these samples are referred to as the Data Simulator (DS).

The same procedure is then applied to reconstructed $\nu_\mu$ CC MC events, the Monte Carlo Simulator (MCS). In order to reduce systematic uncertainties, signal and background efficiencies $\epsilon$ are then obtained from the relation $\epsilon = \epsilon_{\rm MC} \times \epsilon_{\rm DS}/\epsilon_{\rm MCS}$. For selected events, the factor $\epsilon_{\rm DS}/\epsilon_{\rm MCS}$ is within 14% of unity for $\tau$ decay events, but can be as large as 1.8 for background events. [1] The errors on background predictions given in the tables reflect the statistical uncertainties from both MC and DS.

### *4.4 Avoiding biases*

The study of data events in the kinematic region where a signal is expected may introduce biases in the event selection resulting in incorrect background estimates. In order to avoid this problem a procedure referred to as "blind analysis", described in Ref. [1], is used for each $\tau^-$ decay mode. According to this procedure, data events inside the signal region (the "blind region") cannot be analyzed until all the selection criteria are defined and the robustness of the background predictions is demonstrated outside this region. A search for $\bar{\nu}_\mu \to \bar{\nu}_\tau$ oscillations, where no $\tau^+$ signal is expected because of the small $\bar{\nu}_\mu$ content (see Sec. 3), is used as a control sample. The definition of the final cuts is made by optimizing the sensitivity to oscillations. This is defined as the average upper limit on the oscillation probability that would be obtained, in the absence of a signal, by an ensemble of experiments with the same expected background [11]. In general, several independent analyses are performed within the same decay channel. This allows at the same time a further cross-check of results and an upgrade of the $\nu_\tau$ search. The sensitivity to oscillations provides the final criterion for any choice between different analyses or for the replacement of a previous analysis by a newer one. The choice is made before looking at data events falling in the signal region. This rule was strictly applied to each of the changes introduced in the analyses with respect to Ref. [1].

In addition, the final efficiency evaluation for signal and background is performed with fully unbiased MC samples, statistically independent from those used to define the selection criteria.

[1] The net correction factors for total background in each DIS analysis are 1.8 for $\tau^- \to e^-\bar{\nu}_e\nu_\tau$, 1.2 for $\tau^- \to h^-\nu_\tau$, 1.7 for $\tau^- \to \rho^-\nu_\tau$, and 1.4 for $\tau^- \to h^-h^+h^-(n\pi^0)\nu_\tau$.

Table 1
**$\tau^- \to e^-\bar{\nu}_e\nu_\tau$ DIS search**: Number of data events and of the corresponding expected background events (from data sample sizes of Sec. 3) as a funcion of cuts. In the $\nu_\mu$ CC and NC columns, small contributions from $\bar{\nu}$ interactions are included. The corresponding $\tau^- \to e^-\bar{\nu}_e\nu_\tau$ signal efficiency (%) and the effect of the selection on the $\tau^+$ control sample are also shown. The numbers quoted for the initial selection are only partially corrected with the Data Simulator.

| Sample | $\nu_\tau$ CC | $\nu_e$ CC | $\bar{\nu}_e$ CC | $\nu_\mu$ CC | | NC | | Tot Bkgnd | | Data | |
|---|---|---|---|---|---|---|---|---|---|---|---|
| Charge | – | – | + | – | + | – | + | – | + | – | + |
| $e^\pm$ ID | 20.0 | 2710 | 340 | 53 | 149 | 110 | 115 | 2873 | 604 | 2527 | 570 |
| Preselection | 12.9 | 745 | 83 | 37 | 112 | 95 | 101 | 877 | 296 | 874 | 303 |
| $\ln\lambda_e^{NC} > 2.5$ | 9.5 | 454.3 | 49.5 | 4.0 | 30.0 | 3.5 | 4.1 | 461.8 | 83.6 | 464 | 86 |
| $\ln\lambda_e^{CC} > 3.0$ | 3.6 | $5.3 \pm 0.5$ | $0.7 \pm 0.2$ | $0.0^{+0.4}_{-0.0}$ | $3.8 \pm 1.8$ | $0.0^{+0.2}_{-0.0}$ | $3.5 \pm 1.6$ | $5.3^{+0.7}_{-0.5}$ | $8.0 \pm 2.4$ | 5 | 9 |

## 5 $\tau^- \to e^-\bar{\nu}_e\nu_\tau$ DIS channel

The search for $\tau^- \to e^-\bar{\nu}_e\nu_\tau$ proceeds with the preliminary identification of the prompt electron in events with no other prompt leptons, followed by kinematic rejection of backgrounds. The first step is intended to select genuine and well measured electrons whose topology can be efficiently exploited by the kinematic selection.

### *5.1 Prompt electron identification*

The identification of the electron candidate is performed according to strict criteria which were partially improved with respect to those described in Ref. [1]. Primary electrons are defined as DC tracks with $p > 1.5$ GeV/c which are associated to the primary vertex and satisfy requirements based on: TRD identification algorithms [4]; the PS pulse height [5]; the ECAL cluster shape [10]; and consistency between the associated electromagnetic (EM) energy and DC momentum of the candidate. Overall, these requirements achieve a charged pion rejection factor of more than $10^4$.

Secondary electrons from Dalitz decays and from photons converting close to the primary vertex are suppressed by requiring that the candidate electron does not form an invariant mass of less than 50 MeV/$c^2$ with any particle of opposite charge.

These requirements yield an efficiency of 20% for prompt electrons from $\tau^- \to e^-\bar{\nu}_e\nu_\tau$, while accepting only $2.9 \times 10^{-5}$ of $\nu_\mu$ CC and $2.0 \times 10^{-4}$ of neutral currents (line 1 of Table 1).

The selection of $\tau^- \to e^-\bar{\nu}_e\nu_\tau$ decays is performed by constructing likelihood ratios which exploit the full topology of the event. The kinematic variables entering the corresponding pdf's are chosen on the basis of their internal correlations, which are globally taken into account by the likelihood functions.

Events selected at this stage of the analysis are mostly $\nu_e$ CC interactions, with a genuine primary electron, and NC events, with an electron from photon conversion or $\pi^0$ Dalitz decay. In $\nu_e$ CC events the electron is typically well-isolated and balances the momentum of the hadron jet in the transverse plane. On the other hand, in NC interactions the electron is embedded in the hadron jet with transverse momentum almost aligned with it. The signal has intermediate properties between these two extremes since neutrinos carry away transverse momentum and the sizeable $\tau$ mass introduces a component of the electron momentum perpendicular to the $\tau$ direction, thus reducing its isolation.

In order to distinguish the two background sources from signal we implement an event classification with the use of two distinct likelihood functions. The first function is designed to separate signal from NC events:

$$\mathcal{L}_e^{NC} \equiv [[[\theta_{\nu T}, \theta_{\nu H}], \theta_{\tau_V h_i}, Q_T], M_T, E^{\tau_V}]$$

and includes mainly longitudinal variables. This is motivated by the significant contribution of these variables to isolation and by the need to avoid strong biases on the transverse plane which would worsen the $\nu_e$ CC rejection. For each event, a likelihood ratio $\lambda_e^{NC}$ is defined as the ratio of the $\mathcal{L}_e^{NC}$ functions constructed from signal and $NC$ events respectively.

The second function is designed to distinguish signal from $\nu_e$ CC events:

$$\mathcal{L}_e^{CC} \equiv [[Q_{\rm Lep}, \rho_{\tau_V}, \rho_H], E_{\rm vis}, p_T^m, M_T]$$

and primarily includes information on the transverse plane kinematics. In order to reduce systematic effects, the permutation $[[E_{\rm vis}, p_T^m, M_T], Q_{\rm Lep}, \rho_{\tau_V}, \rho_H]$ is also considered. For each event, $\lambda_e^{CC}$ is defined as the minimum value between the likelihood ratios constructed from the two permutations of the $\mathcal{L}_e^{CC}$ function for signal and $\nu_e$ CC events respectively.

The conditions $\phi_{\tau_V H} + \phi_{mH} < 1.96\pi$ and $p_T^{\tau_V} > 0.1$ GeV/$c$ are applied to ensure that the transverse angles are well defined. In addition, a preselection cut $\phi_{mH} > 0.6\pi$ restricts the parameterization of the $\mathcal{L}_e^{NC}$ and $\mathcal{L}_e^{CC}$ functions to the region relevant for the $\tau$ search (line 2 of Table 1).

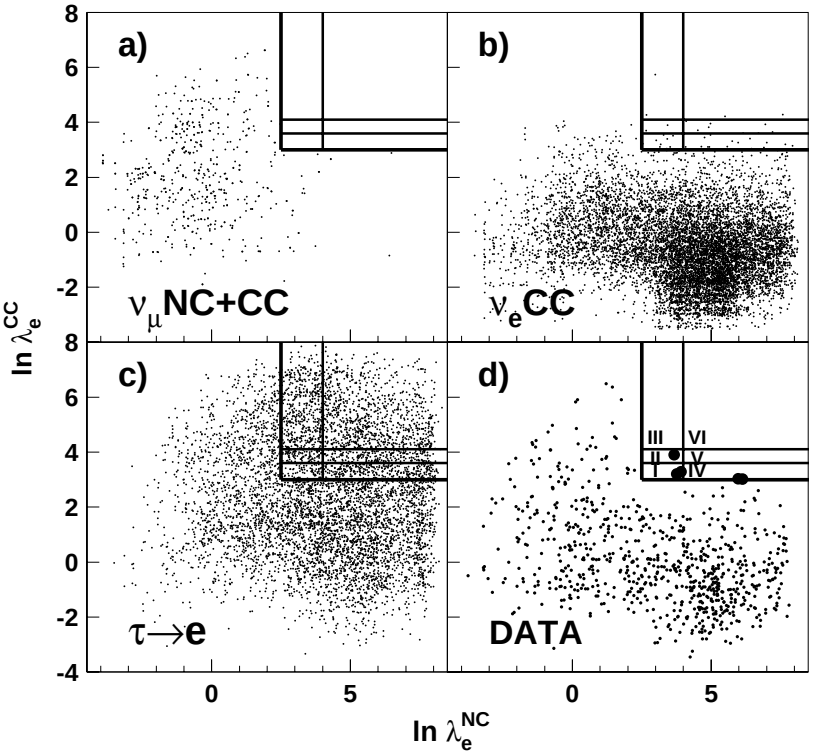


Fig. 1. $\boldsymbol{\tau^- \rightarrow e^-\bar{\nu}_e\nu_\tau}$ **DIS search**: Scatter plot of $\ln\lambda_e^{CC}$ vs $\ln\lambda_e^{NC}$ for a) MC $\nu_\mu$ NC and CC, b) MC $\nu_e$ CC, c) MC $\tau^- \rightarrow e^-\bar{\nu}_e\nu_\tau$ and d) data events. The large box at the upper right corner, divided into six bins, defines the signal region. The five data events falling inside this region are shown as enlarged full circles.

Table 2
$\boldsymbol{\tau^- \rightarrow e^-\bar{\nu}_e\nu_\tau}$ **DIS search**: Number of background and data events in the subdivisions of the signal region (Fig. 1). The corresponding $N_\tau^{\mu\tau}$ and $N_\tau^{e\tau}$, as defined in Sec. 9, are listed in the last two columns. The last two lines define the binning used for the $E_{\rm vis} < 12$ GeV region.

| Analysis | Bin # | Tot bkgnd | Data | $N_\tau^{\mu\tau}$ | $N_\tau^{e\tau}$ |
|---|---|---|---|---|---|
| $\tau^- \rightarrow e^-\bar{\nu}_e\nu_\tau$ DIS | I | $0.85^{+0.26}_{-0.16}$ | 2 | 134 | 2.7 |
| ($E_{\rm vis} > 12$ GeV) | II | $0.46^{+0.23}_{-0.12}$ | 1 | 128 | 2.7 |
| | III | $0.18^{+0.18}_{-0.08}$ | 0 | 639 | 13.8 |
| | IV | $1.85 \pm 0.22$ | 2 | 535 | 12.9 |
| | V | $0.78 \pm 0.15$ | 0 | 389 | 8.4 |
| | VI | $0.16 \pm 0.08$ | 0 | 1388 | 29.8 |
| ($E_{\rm vis} < 12$ GeV) | I+IV+V | $0.77 \pm 0.26$ | 0 | 247 | 2.8 |
| | II+III+VI | $0.27 \pm 0.13$ | 0 | 650 | 8.4 |

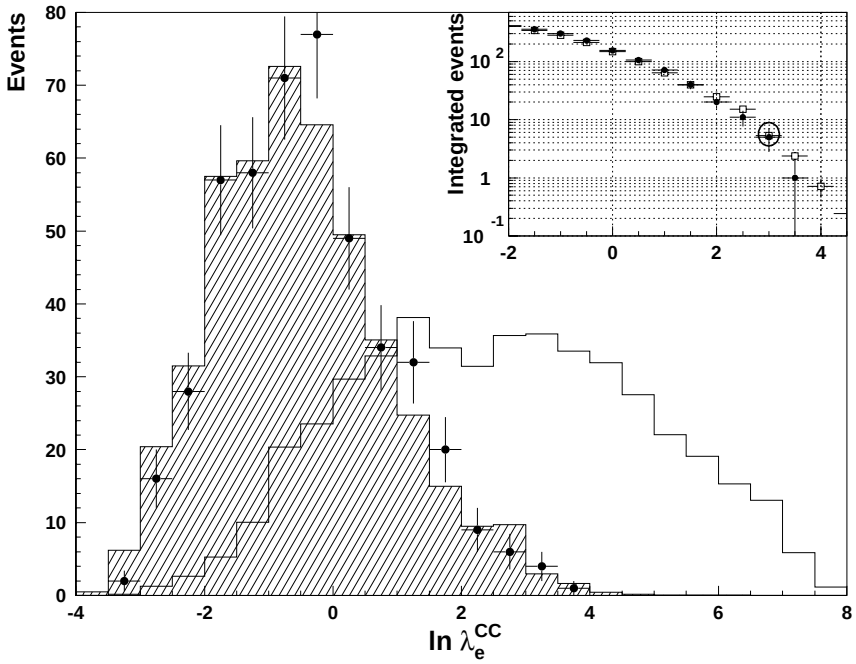


Fig. 2. $\boldsymbol{\tau^- \rightarrow e^-\bar{\nu}_e\nu_\tau}$ **DIS search**: Histogram of $\ln\lambda_e^{CC}$ for events passing all cuts except the cut on $\ln\lambda_e^{CC}$, for data (points with statistical error bars), total backgrounds (shaded) and $N_\tau^{\mu\tau}$ (Sec. 9), scaled down by a factor 20 (unshaded). The inset gives, for each value of $\ln\lambda_e^{CC}$, the total number of events beyond that value, for data (dots) and expected background (squares); the encircled points are at the boundary of the signal region.

The sensitivity is optimized in the plane $[\ln\lambda_e^{NC}, \ln\lambda_e^{CC}]$, which is shown in Figure 1 for simulated signal and backgrounds. A signal region (the blind region), subdivided into six bins, is defined at large values of both $\ln\lambda_e^{NC}$ and $\ln\lambda_e^{CC}$. This corresponds to the selection of events where the electron is isolated from the hadron jet, but does not balance it in the transverse plane. The optimal sensitivity of the analysis lies in a region characterized by less than 0.5 background events (Table 2). In order to increase the sensitivity to oscillations at low $\Delta m^2$ a further binning, defined by a cut at $E_{\rm vis} = 12$ GeV, is considered for the computation of the $\sin^2 2\theta - \Delta m^2$ confidence region.

Data (Fig. 1d) are found to be consistent with background expectations inside the signal region (see Tables 1 and 2). The distribution of $\ln\lambda_e^{CC}$ for data events, passing all the previous cuts, is also in good agreement with background, as can be seen in Figure 2.

## 6 $\tau^- \to h^-(n\pi^0)\nu_\tau$ DIS channel

The search for $\tau^- \to h^-(n\pi^0)\nu_\tau$ decays, where $h^-$ is a hadron and $n \geq 0$, benefits from the large branching ratio of this decay mode. Two independent analyses of the full inclusive sample are separately optimized for the exclusive $\tau^- \to \rho^-\nu_\tau$ and $\tau^- \to h^-\nu_\tau$ topologies.

### *6.1 $\tau^- \to \rho^-\nu_\tau$ search*

The signal search starts with the identification of the $\pi^0$ and $\pi^-$ candidates produced in the $\rho$ decay. Each of the two photons from $\pi^0$ decay can be detected either as neutral electromagnetic clusters or, in case it converts, as two oppositely charged tracks forming a secondary vertex. We thus search for the $\pi^0$ either as two separate photons ($2\gamma$), neutral clusters or conversions, or, in case they coalesce in ECAL, as two overlapped clusters ($1\gamma$). The $1\gamma$ and $2\gamma$ decay topologies are treated as two independent analyses.

#### *6.1.1 Candidate selection*

In each event all the possible $\pi^0$ and $\pi^-$ combinations are considered. In the $2\gamma$ mode a $\pi^0$ candidate is built from two photons with $E > 0.150$ GeV and an invariant mass $0.1 < M_{\gamma\gamma} < 0.180$ GeV/$c^2$. A $\pi^-$ candidate is a DC track with a momentum $p > 1$ GeV/$c$. A $\pi^0\pi^-$ pair is considered as a $\rho$ candidate if it has an invariant mass $0.6 < M_{\pi^0\pi^-} < 0.9$ GeV/$c^2$. In the $1\gamma$ mode a $\pi^0$ is a neutral electromagnetic cluster with $E > 2$ GeV, while a $\pi^-$ candidate is defined as a DC track with $p > 3$ GeV/$c$. The $\rho$ candidates must have an invariant mass $0.4 < M_{\pi^0\pi^-} < 0.9$ GeV/$c^2$. In both topologies, we require that the $\pi^-$ candidate tracks would have reached the muon chambers if they had been muons.

The following likelihood functions are used to select among all the combinations the $\rho$ most likely originating from a $\tau$ decay:

$$\mathcal{L}^S_{\rho,1\gamma} \equiv [E^{\tau_V}/E_{\rm vis}][\theta_{\tau_V H}]; \qquad \mathcal{L}^S_{\rho,2\gamma} \equiv [E^{\pi^0}/E_{\rm vis}, E^{\pi^-}/E_{vis}][\theta_{\tau_V H}]$$

where $E^{\pi^0}$ and $E^{\pi^-}$ are the energies of the $\pi^0$ and of the $\pi^-$ respectively. A likelihood ratio $\lambda^S_\rho$ is built as the ratio of $\mathcal{L}^S_\rho$ for correct and random combinations of $\tau$ decay products. Selecting the maximum likelihood combination results in the correct choice in about 75% of the cases. Signal efficiencies and numbers of expected background events after candidate selection are shown in Table 3 both for $1\gamma$ and $2\gamma$ modes.

Table 3
**$\tau^- \to \rho^- \nu_\tau$ DIS search**: Number of data events and of the corresponding expected background events (from data sample sizes of Sec. 3) as a funcion of cuts for both the $1\gamma$ and $2\gamma$ topologies. In the $\nu_\mu$ CC and NC columns, small contributions from $\bar{\nu}$ interactions are included. The corresponding signal efficiency (%) and the effect of the selection on the $\tau^+$ control sample are also shown. The numbers quoted for the initial selection are only partially corrected with the Data Simulator.

| Sample | | $\nu_\tau$ CC | $\nu_\mu$ CC | | NC | | $\nu_e$ CC | | Tot Bkgnd | | Data | |
|---|---|---|---|---|---|---|---|---|---|---|---|---|
| Charge | | – | – | + | – | + | – | + | – | + | – | + |
| $\rho^\pm$ ID | $1\gamma$ | 11.0 | 3086 | 7107 | 11312 | 10808 | 175 | 265 | 14574 | 18180 | 15777 | 18166 |
| | $2\gamma$ | 8.5 | 4412 | 7295 | 12170 | 11831 | 157 | 258 | 16739 | 19386 | 17369 | 19452 |
| Lepton veto | $1\gamma$ | 5.9 | 434 | 373 | 6792 | 3830 | 30 | 31 | 7256 | 4233 | 7461 | 4553 |
| | $2\gamma$ | 4.5 | 449 | 362 | 6916 | 3924 | 29 | 28 | 7394 | 4314 | 7126 | 4292 |
| $\ln \lambda_\rho^{NC} > 5.0$ | $1\gamma$ | 0.9 | 1.2 | 0.4 | 4.5 | 2.0 | 0.75 | 1.4 | $6.4 \pm 1.9$ | $3.8 \pm 1.2$ | 6 | 4 |
| | $2\gamma$ | 0.3 | 0.8 | 0.4 | 1.8 | 0.6 | 0.5 | 0.74 | $3.1 \pm 1.4$ | $1.8 \pm 0.7$ | 2 | 2 |

### *6.1.2 Rejection of charged current interactions*

A muon veto is implemented using both kinematic criteria and particle identification. We search for the unidentified muon track among the highest $p_T$ track ($p_T^{\rm lead}$), the $\pi^-$ candidate and all the negatively charged tracks fulfilling the requirement $p_T^{\rm lead} - p_T^{\rm track} < 0.2$ GeV/$c$. These tracks are considered muon candidates if $p_T/p > 0.2$. We reject events fulfilling one of the following conditions:

- the highest $p_T$ track does not point to the calorimeter fiducial volume;
- the highest $p_T$ track or the $\pi^-$ candidate deposit ECAL and HCAL signals consistent with that of a minimum ionizing particle;
- any primary track is associated with a signal in the muon chambers;
- any primary track with $p_T^{\rm lead} - p_T^{\rm track} < 0.2$ GeV/c has $p_T/p > 0.3$.

The $\nu_e$ CC interactions containing bremsstrahlung photons not associated with the electron track may closely fake the $\tau \to \rho$ topology. The electron veto used to reduce this background follows the principles of the muon veto: the highest and second highest $p_T$ tracks and the $\pi^-$ candidate are considered candidate electrons. We then reject events fulfilling one of the following requirements:

- one of the candidate electrons has $p_T > 0.6$ GeV/$c$ and is identified by ECAL, PS or TRD algorithms;
- the transverse momentum of the highest $p_T$ particle, charged or neutral, built collecting all the photons in a vertical bremstrahlung strip [1] is larger than 2.5 $GeV/c$.
- the $\pi^-$-$\gamma$ opening angle in the $1\gamma$ topology is smaller than 0.02 rad;

A further cut, $p_T^m > 0.4$ GeV/$c$, is applied to reject both $\nu_\mu$ CC and $\nu_e$ CC events. The effect of the lepton veto is shown in Table 3.

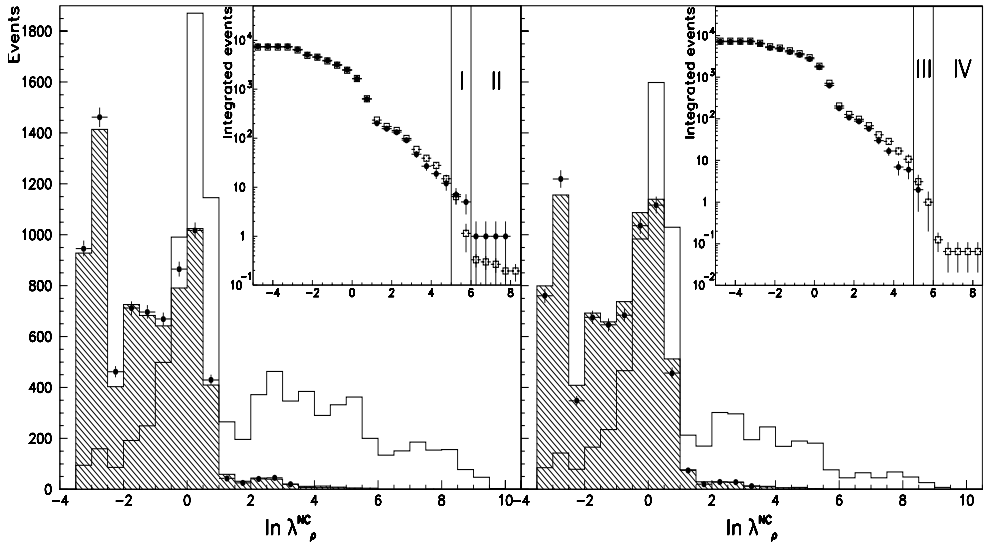


Fig. 3. $\boldsymbol{\tau^- \to \rho^- \nu_\tau}$ **DIS search**: Histogram of $\ln \lambda_\rho^{NC}$ for events passing all cuts except the cut on $\ln \lambda_\rho^{NC}$, for data (points with statistical error bars), total backgrounds (shaded) and $N_\tau^{\mu\tau}$ (Sec. 9), scaled down by a factor 2 (unshaded). Results from both the $1\gamma$ (left) and the $2\gamma$ (right) topologies are shown. The insets give, for each value of $\ln \lambda_\rho^{NC}$, the total number of events beyond that value, for data (dots) and expected background (squares); the vertical lines define the four subdivisions of the signal region.

*6.1.3 Rejection of neutral current interactions*

The rejection of neutral current interactions is accomplished by using the likelihood function defined as :

$$\mathcal{L}_\rho^{NC} \equiv [[[\theta_{\nu T}, \theta_{\nu H}], \theta_{\tau_V H}, Q_T], \phi_{\tau_V H}, p_{T\,||}^m]$$

This function is similar to $\mathcal{L}_e^{NC}$ since most of the kinematic criteria used to reject NC interactions are independent of the particular decay channel. For each event, a likelihood ratio $\lambda_\rho^{NC}$ is defined as the ratio of the $\mathcal{L}_\rho^{NC}$ functions constructed from signal and $NC$ events respectively.

The condition $\ln \lambda_\rho^{NC} > 5$ defines the blind region. In this region two bins for each decay topology ($1\gamma$ and $2\gamma$) are considered. Events selected in both the $1\gamma$ and $2\gamma$ topologies are assigned to the more sensitive bin. The optimal sensitivity is reached in those bins where the expected background is $< 0.5$ events (Table 4). In addition to the standard control samples (Sec. 4.4) a further control sample is defined selecting $\rho$ candidates with mass lying in the sideband of the $M_{\pi^0\pi^-}$ invariant mass distribution. All background predictions on the control samples have shown good agreement with data.

Finally, the data inside the blind region are found to be consistent with back-

Table 4
**$\tau^- \to h^-(n\pi^0)\nu_\tau$ DIS search**: Number of background and data events in the signal region for both the $\tau \to \rho$ and $\tau \to h$ topologies. The corresponding $N_\tau^{\mu\tau}$ and $N_\tau^{e\tau}$, as defined in Sec. 9, are listed in the last two columns. The last line refers to the overlap bin, as described in Sec.6.3.

| Analysis | | | Bin # | Tot bkgnd | Data | $N_\tau^{\mu\tau}$ | $N_\tau^{e\tau}$ |
|---|---|---|---|---|---|---|---|
| $\tau \to h(n\pi^0)$ | DIS | $\rho$ | I $1\gamma$ | $6.10 \pm 1.93$ | 5 | 883 | 20.5 |
| | | $\rho$ | II $1\gamma$ | $0.33^{+0.74}_{-0.10}$ | 0 | 1736 | 41.9 |
| | | $\rho$ | III $2\gamma$ | $3.00 \pm 1.40$ | 2 | 466 | 10.5 |
| | | $\rho$ | IV $2\gamma$ | $0.06^{+0.88}_{-0.04}$ | 0 | 222 | 5.3 |
| $\tau \to h(n\pi^0)$ | DIS | h | I | $4.4 \pm 1.9$ | 3 | 817 | 18.3 |
| | | h | II | $2.4 \pm 0.8$ | 2 | 1205 | 25.5 |
| $\tau \to h(n\pi^0)$ | DIS | $h/\rho$ | – | $0.0^{+0.74}_{-0.0}$ | 1 | 210 | 5.0 |

ground expectations (Figure 3). The number of events found in each bin is listed in Table 4.

### *6.2 $\tau^- \to h^-\nu_\tau$ search*

The $h^-$ candidate is the highest $p_T$ negative primary track, provided it is one of the two highest $p_T$ tracks of either charge in the event. It is then required that this candidate is not identified as a muon or an electron, that it is associated with an energy deposition in ECAL and that $3 < p^{\tau_V} < 150$ GeV/c (line 1 of Table 5).

The lepton veto against CC background, described in Ref. [1], is similar to that used in the $\tau^- \to \rho^-\nu_\tau$ search. This is based on particle identification criteria which are applied both to the $h^-$ candidate and to primary tracks with $p_T > 0.8$ GeV/$c$ (line 2 of Table 5).

After the lepton veto there is still a residual background from $\nu_\mu$ CC interactions in which the outgoing $\mu^-$ is selected as the $h^-$ because it either decayed in flight or suffered a highly inelastic interaction in the calorimeters. This happens in about $10^{-4}$ of all $\nu_\mu$ CC events, as measured by studying a large sample of muons originating from a nearby test-beam and crossing the NOMAD detector [1]. These events are rejected by using the likelihood function :

$$\mathcal{L}_\pi^{CC} \equiv [Q_T, \rho_{\tau_V}, \rho_H]$$

The likelihood ratio $\lambda_\pi^{CC}$ is defined as the ratio of $\mathcal{L}_\pi^{CC}$ for simulated $\tau \to \pi$ signal and $\nu_\mu$ CC data events. Events with $\ln \lambda_\pi^{CC} > -4$ are selected. At

Table 5
**$\tau \rightarrow h^- \nu_\tau$ DIS search**: Number of data events and of the corresponding expected background events (from data sample sizes of Sec. 3) as a funcion of cuts. In the $\nu_\mu$ CC and NC columns, small contributions from $\bar{\nu}$ interactions are included. The corresponding signal efficiency (%) and the effect of the selection on the $\tau^+$ control sample are also shown. The numbers quoted for the initial selection are only partially corrected with the Data Simulator.

| Sample | $\nu_\tau$ CC | $\nu_\mu$ CC | | NC | | $\nu_e$ CC | | Tot Bkgnd | | Data | |
|---|---|---|---|---|---|---|---|---|---|---|---|
| Charge | – | – | + | – | + | – | + | – | + | – | + |
| $h^\pm$ ID | 41.0 | 11400 | 18177 | 51896 | 42550 | 4934 | 1795 | 68230 | 62522 | 72685 | 62266 |
| Lepton veto | 17.0 | 4802 | 9974 | 28764 | 24241 | 106 | 194 | 33672 | 34409 | 28697 | 26583 |
| Preselection | 3.8 | 167 | 214 | 5669 | 4260 | 11 | 18 | 5847 | 4492 | 5881 | 4571 |
| $\ln \lambda_\pi^{NC} > 7.2$ | 0.7 | $3.5 \pm 0.8$ | $7.4 \pm 2.1$ | $3.0 \pm 1.9$ | $7.0 \pm 4.0$ | $0.3 \pm 0.1$ | $1.6 \pm 0.2$ | $6.8 \pm 2.1$ | $16.0 \pm 4.0$ | 6 | 19 |

this stage of the analysis a kinematic preselection is applied by requiring that $M_T < 4$ GeV/$c^2$, $p_T^H > 1.3$ GeV/$c$ and $\rho_H < 0.49$ (line 3 of Table 5).

The kinematic rejection of the remaining backgrounds, mainly NC interactions, is achieved with the likelihood function :

$$\mathcal{L}_\pi^{NC} \equiv [Q_T, M_T, \rho_m][y_{Bj}][p_T^H]$$

For each event, a likelihood ratio $\lambda_\pi^{NC}$ is defined as the ratio of the $\mathcal{L}_\pi^{NC}$ functions constructed from the signal and the sum of simulated backgrounds respectively. The condition $\ln \lambda_\pi^{NC} > 7.2$ singles out the signal region, which is further subdivided in two bins (Table 4).

The number of data events found inside the signal region is consistent with background predictions (Tables 5 and 4).

### *6.3 Combined search*

We combine the two independent analyses of the $\tau^- \rightarrow h^-(n\pi^0)\nu_\tau$ sample into a single inclusive search. The overlap between them is small, mainly due to the isolation condition of the candidate with respect to the hadronic system, which in the $\tau^- \rightarrow h^-\nu_\tau$ search does also include the photons from $\pi^0$ decays. The fraction of the events selected by both analyses is estimated to be 9% for the signal sample and is negligible within the available statistics for the background samples. Events selected in both searches are included into a separate signal bin ($h/\rho$) as shown in Table 4. This statistical treatement provides the best overall sensitivity to oscillations. The upper error on the background estimation for the overlap bin in Table 4 takes into account the limited MC statistics available and the corresponding data simulator correction.

## 7 $\tau^- \to h^-h^+h^-(n\pi^0)\nu_\tau$ DIS channel

The $\tau^- \to h^-h^+h^-(n\pi^0)\nu_\tau$ channel is characterized by the presence of additional constraints due to the internal $3h$ structure. This search is optimized for the $\pi^-\pi^+\pi^-\nu_\tau$ decay, which is dominated by the chain $\tau^- \to a_1^-(1260)\ \nu_\tau \to \rho^0(770)\pi^-\ \nu_\tau \to \pi^-\pi^+\pi^-\ \nu_\tau$. Both the candidate selection and the final background rejection are based upon the artificial neural network technique.

### *7.1 Candidate selection*

The choice of the $3\pi$ system most likely produced by a $\tau$ decay is obtained by using an ANN (*JetNet 3.5* [12]). A three layered *feed-forward* network is implemented with 13 neurons in the input layer, 20 neurons in the hidden layer and a single neuron in the output layer. The expected value for the output neuron, $\mathcal{O}^S_{3\pi}$, is 1 when the correct $\tau$ decay products are selected and 0 otherwise. The input variables are chosen in order to exploit both the internal structure and the global kinematics of the $3\pi$ combinations. The variables related to the internal structure are: the $\pi^-\pi^+\pi^-$ invariant mass $M_{3\pi}$; the two possible $\pi^+\ \pi^-$ invariant masses $M_{\pi^+\pi^-}$; and $\theta_{max}$ and $\theta_{min}$, which are the maximum and the minimum opening angles between the three pions. The event kinematics is described by the set of variables $(\theta_{\nu H}, Q_{Lep}, \rho_{\tau_V}, \rho_H, \rho_m, p^{\tau_V}, p^H, p^{\tau_V}/E_{\rm vis})$. The network is trained on correct and random combinations of the $\tau$ decay products using the *back-propagation* learning algorithm. According to this method, each event is fed to the network several times with successive adjustments of the network parameters to artificially enlarge the training sample. The selection of the $\tau$ daughter candidate as the $3\pi$ combination with the highest $\mathcal{O}^S_{3\pi}$ results in the correct choice in 73% of the cases.

### *7.2 Rejection of charged current interactions*

Charged current events where the lepton escapes particle identification and a random combination of the $3\pi$ is selected are particularly dangerous since the corresponding kinematics are similar to that of the signal. For this reason, a lepton veto is required in addition to the ANN kinematic selection. This is achieved in two steps, referred to as *loose* and *tight* vetos. In the *loose veto* primary leptons identified by the muon stations or by combined TRD, PS and ECAL algorithms are rejected. The *tight veto*, based on kinematic criteria, rejects events where the highest or the second highest $p_T$ tracks have $p_T/p > 0.2$. The training of the ANN used for the final background rejection is performed before the *tight veto* is applied in order to guarantee large training samples. The effect of both vetoes is shown in Table 6.

The final rejection of both CC and NC interactions is achieved with the use of a single three layered feed-forward network. Its architecture is formed by 13 neurons in the input layer, 20 neurons in the hidden layer and one output node whose target value, $\mathcal{O}^B_{3\pi}$, is 0 for background and 1 for signal events. The event kinematics of signal and backgrounds are described by the following set of variables : $(\theta_{\nu T}, \theta_{\nu H}, \theta_{\tau_{\rm V} H}, Q_T, \hat{\nu}, \hat{\mu}, p^{\tau_{\rm V}}, E_{\rm vis}, p^{\tau_{\rm V}}/E_{\rm vis})$. In addition, the variables $(M_{3\pi}, \theta_{min}, \theta_{max}, \mathcal{O}^S_{3\pi})$ are also used as an input to the network. This exploits the discriminating power that the $3\pi$ internal structure can still provide. The training of the network proceeds in the same way as for the $3\pi$-ID network.

The blind region is defined by $\mathcal{O}^B_{3\pi} > 0.97$. Since no significant variation of the signal-to-background ratio is observed inside this region, no binning is used in this channel. The distribution of $\mathcal{O}^B_{3\pi}$ for data events, passing all the previous cuts, is in good agreement with background predictions (Figure 4), thus providing no evidence for oscillations. The number of data events falling in the blind region is given in Table 6.

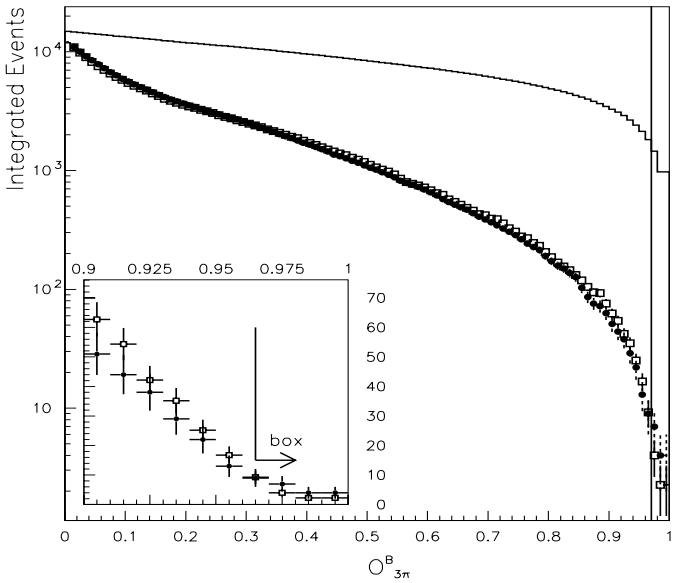


Fig. 4. $\boldsymbol{\tau^- \to h^- h^+ h^- (n\pi^0)\nu_\tau}$ **DIS search**: Total number of events passing cut as a function of a cut on $\mathcal{O}^B_{3\pi}$ for data (dots), total backgrounds (squares) and $N^{\mu\tau}_\tau$ (histogram), as defined in Section 9. The signal region is at the right of the vertical line.

Table 6
**$\tau^- \to h^-h^+h^-(n\pi^0)\nu_\tau$ DIS search**: Number of data events and of the corresponding expected background events (from data sample sizes of Sec. 3) as a funcion of cuts. In the $\nu_\mu$ CC and NC columns, small contributions from $\bar{\nu}$ interactions are included. The corresponding signal efficiency (%) and the effect of the selection on the $\tau^+$ sample are shown. The numbers quoted for the initial selection are only partially corrected with the Data Simulator.

| Sample | $\nu_\tau$ CC | $\nu_\mu$ CC | | $\nu_e$ CC | | NC | | Tot Bkgnd | | Data | |
|---|---|---|---|---|---|---|---|---|---|---|---|
| Charge | – | – | + | – | + | – | + | – | + | – | + |
| Pre-selection | 56.0 | 97861 | 99385 | 2904 | 3153 | 144496 | 125400 | 245261 | 227938 | 216988 | 244010 |
| Loose veto | 44.0 | 49736 | 48856 | 1349 | 1330 | 84403 | 82308 | 135488 | 132494 | 119991 | 132104 |
| Tight veto | 15.0 | 1656 | 1881 | 150 | 149 | 10450 | 11941 | 12256 | 13971 | 12397 | 12681 |
| $\mathcal{O}^B_{3\pi} > 0.97$ | 1.9 | 2.2±1.0 | 1.3±0.9 | 0.7±0.2 | 0.8±0.2 | 6.7±2.2 | 4.8±3.2 | 9.6±2.4 | 6.9±3.3 | 9 | 6 |

## 8 Low Multiplicity topologies

In order to optimize the sensitivity to oscillations at low $\Delta m^2$ an independent analysis of the LM events is performed for each $\tau$ decay channel. The condition $p_H < 1.5$ GeV/c enriches the LM sample in quasi-elastic (QE) and resonance (RES) events, avoiding double counting with the corresponding DIS searches. Overall, the QE and RES events represent 6.3% of the total $\nu_\mu CC$ interactions at the available neutrino energies. The topology of LM events simplifies the reconstruction and the selection criteria in this kinematic region, which is also characterized by a more favourable $\sigma_\tau/\sigma_\mu$ cross-section ratio (Sec. 9).

The reconstruction and simulation of LM topologies has significantly improved with respect to Ref.[13], leading to more realistic background estimates for these channels and to different selection criteria. Furthermore the LM analyses described in Ref.[13] were only based on about 15% of the full data sample.

### *8.1 $\tau^- \to e^-\bar{\nu}_e\nu_\tau$ LM channel*

The prompt electron identification, similar to that used in the DIS search, is applied to primary DC tracks with $p > 2$ GeV/c and is based on TRD and ECAL information.

Secondary electrons from Dalitz decays and from photons converting close to the primary vertex are suppressed by requiring that the candidate electron not form an invariant mass of less than 200 MeV/$c^2$ with any particle of opposite charge. Furthermore, the candidate must form an angle smaller than 200 mrad with the beam direction. The conditions $M_T < 2$ GeV/c$^2$ and $p_T^{as} < 0.2$ are then applied in order to reject NC interactions. At this stage of the analysis the background consists mostly of $\nu_e$ CC interactions, which are suppressed

Table 7
**$\tau^- \to e^-\bar{\nu}_e\nu_\tau$ LM search**: Number of background and data events in the three bins of the signal region. The corresponding $N_\tau^{\mu\tau}$ and $N_\tau^{e\tau}$, as defined in Sec. 9, are listed in the last two columns.

| Analysis | | Bin # | Tot bkgnd | Data | $N_\tau^{\mu\tau}$ | $N_\tau^{e\tau}$ |
|---|---|---|---|---|---|---|
| $\tau^- \to e^-\bar{\nu}_e\nu_\tau$ | LM | I | $3.09 \pm 0.67$ | 3 | 282 | 2.8 |
| | | II | $1.50 \pm 0.41$ | 2 | 285 | 2.8 |
| | | III | $0.82 \pm 0.41$ | 1 | 292 | 2.9 |

by using the likelihood function:

$$\mathcal{L}^{CC}_{e,LM} \equiv [p_T^{as}, p_T^m][p^{\tau_V}]$$

For each event, a likelihood ratio $\lambda^{CC}_{e,LM}$ is defined as the ratio of the $\mathcal{L}^{CC}_{e,LM}$ functions constructed from signal and $\nu_e$ CC events, respectively. The signal region starts at $\ln\lambda^{CC}_{e,LM} > 0.8$ and is further subdivided into three bins (Table 7). Data events populate the blind region consistently with background expectations in all bins (Table 7).

### *8.2 $\tau^- \to h^-(n\pi^0)\nu_\tau$ LM channel*

As for the DIS search, two independent analyses of the full inclusive sample are separately optimized for the exclusive $\tau^- \to \rho^-\nu_\tau$ and $\tau^- \to h^-\nu_\tau$ topologies. Events common to both analyses are negligible in the LM sample since the $p^H$ cut suppresses events with large neutral activity.

#### *8.2.1 $\tau^- \to \rho^-\nu_\tau$ search*

The $\pi$ produced in the $\rho$ decay is defined as the primary DC track with the highest momentum in the event, pointing to ECAL and having $p > 3$ GeV/c. The $\pi^0$ candidate is formed with $\gamma$'s which can be either neutral ECAL clusters of $E > 200$ MeV or photons converted in the DC volume. When different $\pi^0$ combinations are possible, the one with the highest momentum and $90 < M_{\pi^0} < 200$ MeV/c$^2$ is chosen. Moreover, the $\rho$ invariant mass must satisfy $0.58 < M_\rho < 1.0$ GeV/c$^2$. A lepton veto is then applied by requiring that no primary electron be present and that the $\pi$ candidate not be consistent with being a muon or an electron. The background at this level is dominated by NC interactions, which are rejected by the cut $1.0 < M_T < 2.0$ GeV/$c^2$ and by the use of the likelihood function :

$$\mathcal{L}^{NC}_{\rho,LM} \equiv [\theta_{\tau_V H}, p^{\tau_V}]$$

A likelihood ratio $\lambda^{NC}_{\rho,LM}$ is computed as the ratio of the $\mathcal{L}^{NC}_{\rho,LM}$ functions constructed from signal and NC events respectively. Data events inside the blind region, starting at $\ln\lambda^{NC}_{\rho,LM} > 1.8$, are found to be consistent with background expectations (Table 8). Since no significant variation of the signal-to-background ratio is observed inside the signal region no further binning is used.

### *8.2.2 $\tau^- \to h^-\nu_\tau$ search*

The $\tau^- \to h^-\nu_\tau$ LM search follows closely the analysis flow of the corresponding $\tau^- \to \rho^-\nu_\tau$ LM search. The DC track with the highest momentum in the event, pointing to ECAL and having $p > 3$ GeV/c is the $h^-$ candidate. A lepton veto on the candidate track and the requirement $1.0 < M_T < 2.0$ GeV/c$^2$ are then applied. The final background, mostly NC interactions, is rejected with the likelihood function $\mathcal{L}^{NC}_{\pi,LM} \equiv \mathcal{L}^{NC}_{\rho,LM}$. A likelihood ratio $\lambda^{NC}_{\pi,LM}$ is computed as the ratio of the $\mathcal{L}^{NC}_{\pi,LM}$ functions constructed from signal and NC events respectively. The signal region is defined at $\ln\lambda^{NC}_{\pi,LM} > 2.0$. Data events inside this blind region are found to be consistent with background expectations (Table 8). Since no significant variation of the signal-to-background ratio is observed inside the signal region no further binning is used.

## *8.3 $\tau^- \to h^-h^+h^-(n\pi^0)\nu_\tau$ LM channel*

In each event, the signal search starts with the identification of all the possible $\pi^-\pi^+\pi^-$ combinations with $0.4 < M_{3\pi} < 1.6$ GeV/$c^2$. A likelihood function, $\mathcal{L}^{S}_{3\pi,LM}$, is then used to select the $3\pi$ most likely to originate from a $\tau$ decay:

$$\mathcal{L}^{S}_{3\pi,LM} \equiv [p^{\tau_V}, \theta_{\nu\tau_V}][(p^{\pi^-}_1 - p^{\pi^-}_2)/p^{\tau_V}, p^{\pi^+}/p^{\tau_V}][M_1, M_2][\theta_{\tau_V H}]$$

where $p^{\pi^-}_1$ ($p^{\pi^-}_2$) is the highest (lowest) momentum of the two $\pi^-$'s and $M_1$ ($M_2$) is the corresponding invariant mass with the $\pi^+$. A likelihood ratio, $\ln\lambda^{S}_{3\pi,LM}$, is computed as the ratio of the $\mathcal{L}^{S}_{3\pi,LM}$ functions for correct and random combinations of $\tau$ decay products. Selecting the maximum likelihood combination results in the correct choice in 89% of the cases. Moreover, the invariant masses of the two $\pi^+\pi^-$ combinations must be $0.4 < M_{1(2)} < 1.2$ GeV/$c^2$. In order to reduce the background from CC interactions a lepton veto based on particle identification is applied to each of the $3\pi$ tracks, together with the requirement that the $\pi^-$'s have $p^{\pi^-}_{1(2)} > 2.5$ GeV/c. In addition, since in $\nu_\tau$ QE and RES interactions only positively charged hadrons are produced, we reject events where a negative track is present within the hadronic system. The final rejection of NC interactions is achieved with the likelihood function:

$$\mathcal{L}^{NC}_{3\pi,LM} \equiv [M_T, p^{as}_T]\ \mathcal{L}^{S}_{3\pi,LM}$$

Table 8
Summary of backgrounds and efficiencies for all the individual $\tau$ searches. The column $\tau^-$ summarizes the observed number of $\tau^-$ candidate events (Obs.) and the corresponding predicted background (Tot Bkgnd) in the signal region. The column $\tau^+$ contains the equivalent numbers for the positive control sample. The corresponding $\tau^-$ selection efficiencies ($\epsilon$), the $\tau$ branching ratios ($Br$), and the $N_\tau^{\mu\tau}$ and $N_\tau^{e\tau}$ (see text) are also listed.

| Analysis | | | $\tau^-$ | | $\tau^+$ | | | | | |
|---|---|---|---|---|---|---|---|---|---|---|
| | | | Obs. | Tot Bkgnd | Obs. | Tot Bkgnd | $\epsilon(\%)$ | $Br(\%)$ | $N_\tau^{\mu\tau}$ | $N_\tau^{e\tau}$ |
| $\tau \to e$ | | DIS | 5 | $5.3^{+0.7}_{-0.5}$ | 9 | $8.0 \pm 2.4$ | 3.6 | 17.8 | 4110 | 81.5 |
| $\tau \to h(n\pi^0)$ | $\rho$ | DIS | 7 | $9.5 \pm 2.5$ | 6 | $5.6 \pm 1.5$ | 1.04 | 49.8 | 3307 | 78.2 |
| | $h$ | DIS | 5 | $6.8 \pm 2.1$ | 19 | $16.0 \pm 4.0$ | 0.63 | 49.8 | 2022 | 43.7 |
| | $h/\rho$ | DIS | 1 | $0.0^{+0.74}_{-0.0}$ | | | 0.07 | 49.8 | 210 | 5.0 |
| $\tau \to 3h(n\pi^0)$ | | DIS | 9 | $9.6 \pm 2.4$ | 6 | $6.9 \pm 3.3$ | 1.9 | 15.2 | 1820 | 42.6 |
| $\tau \to e$ | | LM | 6 | $5.4 \pm 0.9$ | 3 | $2.2 \pm 0.5$ | 6.3 | 17.8 | 859 | 8.5 |
| $\tau \to h(n\pi^0)$ | $\rho$ | LM | 7 | $5.2 \pm 1.8$ | 21 | $22.2 \pm 6.6$ | 1.02 | 49.8 | 458 | 8.4 |
| | $h$ | LM | 5 | $6.7 \pm 2.3$ | 19 | $21.9 \pm 6.4$ | 0.84 | 49.8 | 357 | 7.2 |
| $\tau \to 3h(n\pi^0)$ | | LM | 5 | $3.5 \pm 1.2$ | 1 | $2.2 \pm 1.1$ | 2.0 | 15.2 | 288 | 4.8 |

A likelihood ratio, $\ln \lambda^{NC}_{3\pi,LM}$, is computed as the ratio of the $\mathcal{L}^{NC}_{3\pi,LM}$ functions constructed from signal and NC events, respectively. The signal region starts at $\ln \lambda^{NC}_{3\pi,LM} > 6.0$ and no further binning is used since there is no significant variation of the signal-to-background ratio. Data events populate the blind region consistently with background expectations (Table 8).

## 9 Results

The final result of the measurement is expressed as a frequentist confidence interval [11] which accounts for the fact that each $\tau$ decay mode and signal bin may have a different signal to background ratio. The acceptance region of Ref. [11] therefore becomes multi-dimensional to contain each of the separate measurements. This computation takes into account the number of observed signal events, the expected background and its uncertainty, and the value of expected signal events if the oscillation probability, $P_{osc}$, were unity [1]. For the $\nu_\mu \to \nu_\tau$ oscillation this last quantity is defined by:

$$N_\tau^{\mu\tau} = N_\mu^{\rm obs} \times (\sigma_\tau/\sigma_\mu) \times Br \times (\epsilon_\tau/\epsilon_\mu) \qquad (1)$$

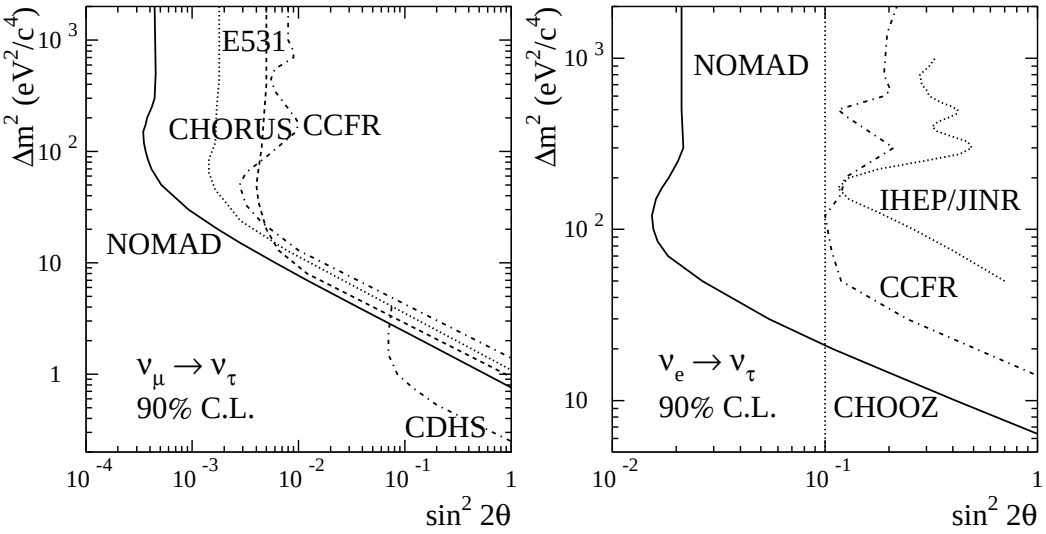


Fig. 5. Contours outlining a 90 % CL region in the $\Delta m^2 - \sin^2 2\theta$ plane for the two-family oscillation scenario. The NOMAD $\nu_\mu \rightarrow \nu_\tau$ (left) and $\nu_e \rightarrow \nu_\tau$ (right) curves are shown together with the limits published by other experiments [15,16].

where:

- $N_\mu^{\rm obs}$ is the observed number of $\nu_\mu$ CC interactions, for the given efficiency $\epsilon_\mu$ (Sec. 1). The number of $\nu_\mu$ CC interactions corresponding to the LM topologies are estimated to be 11% of the total.
- $\epsilon_\tau$ and $\epsilon_\mu$ are the detection efficiencies for $\tau$ signal events and $\nu_\mu$ CC normalization events. The cuts used to select $N_\mu^{\rm obs}$ and $\epsilon_\mu$ vary from channel to channel in order to reduce systematic uncertainties in the ratio $\epsilon_\tau/\epsilon_\mu$ for that channel. For the LM topologies $\epsilon_\tau$ is the average efficiency for QE and RES interactions.
- $\sigma_\tau/\sigma_\mu$ is the suppression factor of the $\nu_\tau$ cross section due to the difference between the $\tau$ and $\mu$ masses, which, for the given $\nu_\mu$ spectrum and the large $\Delta m^2$ hypothesis, is evaluated to be 0.48, 0.60 and 0.82 for the deep inelastic, resonance and quasi-elastic processes. The resulting average values for the DIS and LM analyses are 0.48 and 0.57 respectively.
- $Br$ is the branching ratio for the considered $\tau$ decay channel.

The corresponding maximal number of signal events for the $\nu_e \rightarrow \nu_\tau$ hypothesis, $N_\tau^{e\tau}$, is obtained from $N_\tau^{\mu\tau}$ by reweighting the simulated signal events for the $\nu_e$ to $\nu_\mu$ flux ratio [2]. Table 8 summarizes the relevant quantities for the different decay modes.

The overall systematic uncertainty on the background prediction, mainly associated to the data simulator correction procedure, is estimated to be 20%. The corresponding uncertainties on $N_\tau^{\mu\tau}$ and $N_\tau^{e\tau}$ are 10% and 15%, respectively.

The impact of these latter values on the final combined results is negligible [14].

The resulting 90% C.L. upper limit on the two-generation $\nu_\mu \to \nu_\tau$ oscillation probability is:

$$P_{\rm osc}(\nu_\mu \to \nu_\tau) < 2.2 \times 10^{-4} \tag{2}$$

which corresponds to $\sin^2 2\theta_{\mu\tau} < 4.4 \times 10^{-4}$ for large $\Delta m^2$ and to the exclusion region in the $\Delta m^2 - \sin^2 2\theta$ plane shown in Fig. 5. The result is significantly better than the previously published limits [1,15]. The sensitivity [11] of the experiment is $P_{\rm osc} = 4.3 \times 10^{-4}$; this is higher than the quoted confidence limit, since the number of observed events is smaller than the estimated background. In the absence of signal events, the probability to obtain an upper limit of $2.2 \times 10^{-4}$ or lower is 27% (Figure 6).

The resulting 90% C.L. upper limit on the $\nu_e \to \nu_\tau$ oscillation probability is:

$$P_{osc}(\nu_e \to \nu_\tau) \ < \ 1.1 \times 10^{-2} \tag{3}$$

corresponding to $\sin^2 2\theta_{e\tau} < 2.2 \times 10^{-2}$ for large $\Delta m^2$. The exclusion region in the $\Delta m^2 - \sin^2 2\theta$ plane is also shown in Figure 5. The $\nu_e \to \nu_\tau$ sensitivity is $P_{\rm osc} = 2.0 \times 10^{-2}$ and the probability to obtain an upper limit of $1.1 \times 10^{-2}$ or lower is 31% (Figure 6).

## 10 Conclusions

The analysis of the events with both DIS and LM topologies in the 1995, 1996, 1997 and 1998 NOMAD data sets, excludes a region of the $\nu_\mu \to \nu_\tau$ oscillation parameters which limits $\sin^2 2\theta_{\mu\tau}$ at high $\Delta m^2$ to values smaller than $4.4 \times 10^{-4}$ at 90% C.L., and $\Delta m^2$ to values smaller than $\Delta m^2 < 0.8$ eV$^2/c^4$ at $\sin^2 2\theta_{\mu\tau} = 1$. The corresponding excluded region at 90% C.L. for the $\nu_e \to \nu_\tau$ oscillation parameters includes $\sin^2 2\theta_{e\tau} < 2.2 \times 10^{-2}$ at large $\Delta m^2$ and $\Delta m^2 < 6.5$ eV$^2/c^4$ at $\sin^2 2\theta_{e\tau} = 1$. At large $\Delta m^2$ these limits are more than a factor three more stringent than the previously published ones.

## Acknowledgements

We thank the management and staff of CERN and of all participating institutes for their vigorous support of the experiment. Particular thanks are due

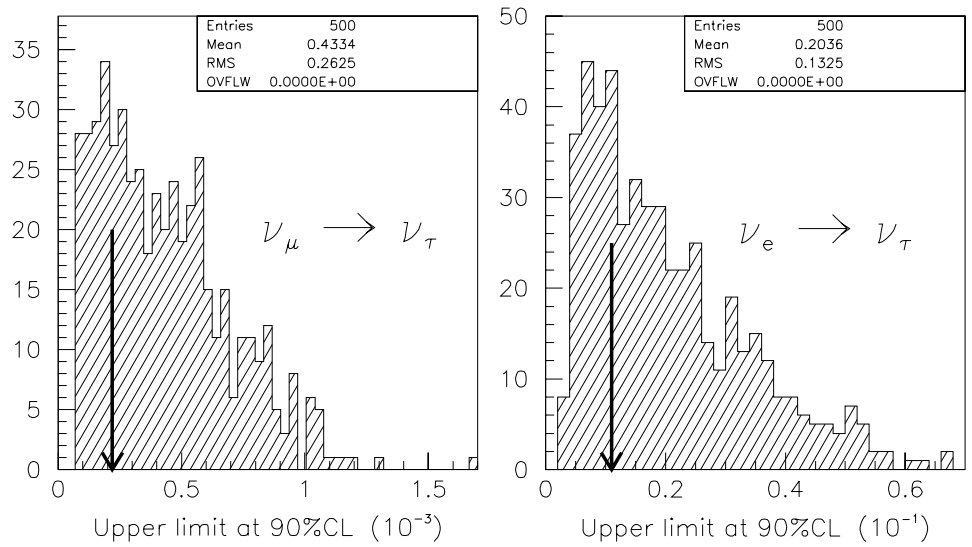


Fig. 6. Histograms of the upper limits obtained, in the absence of signal events, for 500 simulated experiments with the same NOMAD expected background [11]. The averages correspond to the quoted sensitivities while the arrows are the actual upper limits obtained from data in the $\nu_\mu \to \nu_\tau$ (left) and $\nu_e \to \nu_\tau$ (right) searches.

to the CERN accelerator and beam-line staff for the magnificent performance of the neutrino beam. The following funding agencies have contributed to this experiment: Australian Research Council (ARC) and Department of Industry, Science, and Resources (DISR), Australia; Institut National de Physique Nucléaire et Physique des Particules (IN2P3), Commissariat à l'Energie Atomique (CEA), Ministère de l'Education Nationale, de l'Enseignement Supérieur et de la Recherche, France; Bundesministerium für Bildung und Forschung (BMBF, contract 05 6DO52), Germany; Istituto Nazionale di Fisica Nucleare (INFN), Italy; Russian Foundation for Basic Research, Institute for Nuclear Research of the Russian Academy of Sciences, Russia; Fonds National Suisse de la Recherche Scientifique, Switzerland; Department of Energy, National Science Foundation (grant PHY-9526278), the Sloan and the Cottrell Foundations, USA. F.J.P. Soler is supported by a TMR Fellowship from the European Commission.

We also thank our secretarial staff, Jane Barney, Marie-Anne Huber, Rachel Phillips and Mabel Richtering, and the following people who have worked with the collaboration on the preparation and the data collection stages of NOMAD: M. Anfreville, M. Authier, G. Barichello, A. Beer, V. Bonaiti, A. Castera, A. Cavestro, O. Cloué, C. Détraz, L. Dumps, C. Engster, G. Fumagalli, G. Gallay, W. Huta, E. Lessmann, J. Mulon, J.P. Passérieux, P. Petitpas, J. Poinsignon, C. Sobczynski, S. Soulié, L. Visentin, P. Wicht.

## References


[1] NOMAD Collaboration, P. Astier et al., Phys. Lett. B 453 (1999) 169.

[2] NOMAD Collaboration, P. Astier et al., Phys. Lett. B 471 (2000) 406.

[3] NOMAD Collaboration, J. Altegoer et al., Nucl. Instr. and Meth. A 404 (1998) 96.

[4] G. Bassompierre et al., Nucl. Instr. and Meth. A 403 (1998) 363; G. Bassompierre et al., Nucl. Instr. and Meth. A 411 (1998) 63.

[5] D. Autiero et al., Nucl. Instr. and Meth. A 372 (1996) 556; D. Autiero et al., Nucl. Instr. and Meth. A 373 (1996) 358; D. Autiero et al., Nucl. Instr. and Meth. A 387 (1997) 352; D. Autiero et al., Nucl. Instr. and Meth. A 411 (1998) 285.

[6] J. Altegoer et al., Nucl. Instr. and Meth. A 428 (1999) 299-316.

[7] G. Collazuol et al., presented at NOW98 Workshop, Amsterdam, 7-9 September 1998, CERN Preprint OPEN-98-032.

[8] M.C. Gonzales-Garcia, J.J. Gomez-Cadenas, Phys. Rev. D 55 (1997) 1297; B. Van de Vyver, Nucl. Instr. and Meth. A 385 (1997) 91.

[9] C. Albright, R. Shrock, Phys. Lett. B 84 (1979) 123.

[10] D. Autiero et al., Nucl. Instr. and Meth. A 425 (1999) 188.

[11] G.J. Feldman, R.D. Cousins, Phys. Rev. D 57 (1998) 3873.

[12] C. Peterson et al., Comp. Physics Comm. 81 (1994) 185-228.

[13] NOMAD Collaboration, J. Altegoer et al., Phys. Lett. B 431 (1998) 219.

[14] R.D. Cousins, V.L. Highland, Nucl. Instr. and Meth. A 320 (1992) 331.

[15] CHORUS Collaboration, E. Eskut et al., Phys. Lett. B 424 (1998) 202; Phys. Lett B 434 (1998) 205.
E531 Collaboration, N. Ushida et al., Phys. Rev. Lett. 57 (1986) 2897;
CCFR Collaboration, K.S. McFarland et al., Phys. Rev. Lett. 75 (1995) 3993;
CDHS Collaboration, F. Dydak et al., Phys. Lett. B 134 (1984) 281.

[16] CHOOZ Collaboration, M. Apollonio et al., Phys. Lett. B 466 (1999) 415;
CCFR Collaboration, D. Naples et al., Phys. Rev. D 59 (1998);
IHEP/JINR Collaboration, A.A. Borisov et al., Phys. Lett. B 369 (1996) 39.